Journal of Fluorescence, Vol. 10, No. 4, 2000

Vibrational Analysis of the Elpasolites Cs_2NaAlF_6 and Cs_2NaGaF_6 Doped with Cr^{3+} Ions by Fluorescence Spectroscopy

R. J. M. da Fonseca,[1,3] L. P. Sosman,[1] A. Dias Tavares, Jr.,[1] and H. N. Bordallo[2]

Received September 28, 1999; revised May 8, 2000; accepted May 10, 2000

Interest in 3*d* transition metal impurities in ionic crystals has increased due to their important role in the laser activity of these materials. Moreover, recent advances in tunable solid-state lasers and high-power semiconductor laser diode arrays have generated a strong interest in investigating new compounds that emit in the visible and near-infrared spectral regions. In particular, many optical studies have been devoted to Cr^{3+}-doped fluoride crystals as a consequence of the high quality of some Cr^{3+}-based laser materials. In the present investigation, the low-temperature emission spectra of Cr^{3+} ions in the hexagonal elpasolites Cs_2NaAlF_6 and Cs_2NaGaF_6 have been measured. Each compound has two crystallographically inequivalent octahedral sites for the Al^{3+} and Ga^{3+} ions that can be occupied by Cr^{3+} ions. For both materials, the luminescence spectrum presents two zero-phonon lines accompanied by a well-defined vibrational structure. The different peaks of the emission broad band are described in terms of phonons of the lattice and normal modes of the octahedral complex $[CrF_6]^{3-}$. A detailed analysis of the vibrational structure observed leads to the conclusion that the ^2E and $^4T_2$ excited states of the $[CrF_6]^{3-}$ ion are displaced along the e_g and a_{1g} and probably the t_{2g} coordinates.

KEY WORDS: Insulators; crystal and ligand fields; elpasolite; chromium; time-resolved optical spectroscopy.

INTRODUCTION

The interest in developing and investigating new compounds that emit in the visible and near-infrared spectral regions is justified by recent advances in tunable solid-state lasers [1–3]. The drive for new display technologies and the fact that doping ionic crystals within transition metals allows for the tailored design of solid-state laser materials have resulted in a renewed interest in these 3*d* transition metal ion-doped solid-state materials [4,5]. The unfilled 3*d* electronic shell of the transition metal ions has a number of low-lying energy levels, between which the optical transitions can occur and, then, generate the luminescent emission. Since the optically active 3*d* electrons are on the outside of the ions, the spectroscopic properties of the transition metal ions are strongly affected by static and dynamic properties of their environments. So the optical associated spectra are characterized by both sharp and broad emission bands. These broad bands are due to the coupling between electronic transitions and phonons of the host crystal. If, on the one hand, this coupling is interesting for the manufacture of tunable solid-state lasers at room temperature, on the other hand, the extent of a crystal phonon spectrum

[1] Instituto de Física—UERJ, Rua São Francisco Xavier 524, Rio de Janeiro, RJ, 20550-013, Brazil.
[2] IPNS, Argonne National Laboratory, Argonne, Illinois 60439.
[3] To whom correspondence should be addressed at Departamento de Eletrônica Quântica, Instituto de Física, UERJ, Rua São Francisco Xavier 524, 3º andar, Sala D-3030, Maracanã, Rio de Janeiro, RJ, 20550-013, Brazil. e-mail: rauljose@uerj.br

1053-0509/00/1200-0375$18.00/0

favors the nonradiative transitions which greatly reduce the laser efficiency. Consequently, it is interesting to choose materials that have a low cutoff frequency in comparison with the energy gap between the electronic levels of the metal transition ion. In this case, fluoride compounds are promising candidates because they present a cutoff frequency of phonons lower than 600 cm^{-1}.

In the past few years, many spectroscopic studies on the fluoride elpasolites doped with metal transition ions have been reported in the literature [6–9]. Although lasing has been observed for the $3d^1$ (Ti^{3+}), $3d^2$ (Cr^{4+}, Mn^{5+}), $3d^3$ (V^{2+}, Cr^{3+}), $3d^4$ (Cr^{2+}), $3d^6$ (Fe^{2+}), $3d^7$ (Co^{2+}), and $3d^8$ (Ni^{2+}) configurations, undoubtely, Cr^{3+} has been the major 3*d* ion in the development of solid-state laser materials. In a previous work [10,11], the radiative transitions and quantum efficiencies of Cr^{3+} ions associated with different sites in Cs_2NaGaF_6 and Cs_2NaAlF_6 single crystals were investigated by fluorescence spectroscopy. These hosts have the rhombohedral 12L-type crystal structure and belong to the $R\bar{3}m$ space group [12]. The Na^+ and Ga^{3+}/Al^{3+} cations are ordered and octahedrally surrounded by F^- anions. For each material, there are two crystallographically inequivalent trivalent sites for Ga^{3+}/Al^{3+} ions. One site, which we named site I, is characterized by units of (GaF_6) or (AlF_6) linked to two octahedra of (NaF_6) by faces (see Fig. 1). Site II is similar to site I except that the octahedra are linked by corners [5,13]. In the doped material, the Cr^{3+} ions (ionic radius $r = 0.63$ Å) enter these sites, substitutionally replacing the Ga^{3+} ($r = 0.62$ Å) or Al^{3+} ($r = 0.53$ Å) ions.

The analysis of different peaks of the emission broad band in terms of phonons of the lattice and normal modes of the octahedral complex $[CrF_6]^{3-}$ is interesting for the existence of two nonequivalent sites, as mentioned previously. For that reason, we present a detailed analysis of the vibrational structure of those samples. From observed spectra, we have identified the values of the internal vibrational modes for each Cr^{3+} site in CS_2NaGaF_6 and CS_2NaAlF_6.

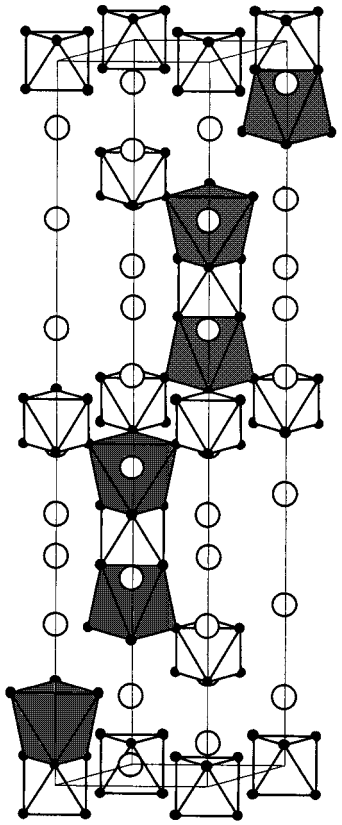

Fig. 1. A polyhedral representation showing the connectivity between the AlF_6 (or GaF_6) and the NaF_6 octahedra. The white and gray polyhedra represent AlF_6 (or GaF_6) and NaF_6, respectively, while the white and black atoms correspond to cesium and fluorine. Some of the octahedra have been removed for clarity.

EXPERIMENTAL

Single crystals of $Cs_2NaGa_{1-x}Cr_xF_6$ and $Cs_2NaAl_{1-x}Cr_xF_6$ with the nominal concentration $x = 0.005$ were obtained by the hydrothermal technique [14]. The fluorides were synthesized by a direct temperature-gradient method as a result of the reaction of aqueous solutions of CsF (30–35 mol%) and NaF whose mole ratio of CsF/NaF changed from 4.8 to 5.2 with appropriate mixtures of oxides Ga_2O_3 and Cr_2O_3 (99.995% pure) at a temperature of about 750 K, a temperature gradient of about 2 K/cm, and pressures of 100–150 MPa. For the hydrothermal experiments autoclaves with copper liners having a volume of about 40 cm^3 were utilized. Under these conditions spontaneously nucleated crystals up to 0.5 cm^3 in size were grown in the upper region of the autoclave. The phase homogeneity of the obtained crystals and the perfection of the crystal lattice were tested by the X-ray powder diffraction method [15]. For spectroscopic investigations, the unoriented platelets of the crystals were used.

High-resolution emission measurements at liquid helium temperature were done, after excitation by the 632.8-nm line of a 5-mW He–Ne laser, with a 2061 MacPherson spectrometer equipped with an RCA C31034-128 photomultiplier and interfaced to a microcomputer. The 4.2 K emission spectra were obtained with an average resolution of 1 cm^{-1}. A Janis ST-100 gas flow cryostat was used in these measurements. Moreover, time-resolved spectra were measured with the phase shift experimental technique [16].

RESULTS AND DISCUSSION

Impurities in crystals, besides interacting with the crystal field, may also interact with the vibrations of the lattices in which they are imbedded. This interaction is commonly represented as arising from a cluster of ions next to the impurity [17]. Then, in the $Cs_2NaGaF_6:Cr^{3+}$ and $Cs_2NaAlF_6:Cr^{3+}$ systems the wave functions of the Cr^{3+} central ion overlap with the wave functions of the six F^- nearly surrounding neighbors. This overlapping is represented, in the simplest form, by a wave function that can be written as the combination of Cr^{3+} plus F^- contributions, which form the molecular orbital for the $[CrF_6]^{3-}$ complex. This molecular orbital is created by the Cr^{3+} atomic orbital, $3d(t_{2g}, e_g)$, $4s(a_{1g})$, and $4p(t_{1u})$, and the anion ligand orbital, $2p_\sigma(a_{1g}, t_{1u}, e_g)$ and $2p_\pi(t_{1u}, t_{2g}, t_{2u}, t_{1g})$. In the O_h group, it can also be represented by $\Gamma^{vib} = a_{1g} + e_g + t_{2g} + 2t_{1u} + t_{2u}$. This orbital admixture is more significant for the Cr^{3+} ion than other $3d$ ions because of its stronger covalence [8]. In this section, the analysis of the results is based on the position and intensity mechanism of the vibronic lines, and many of the vibrational assignments are made in analogy with prior work in the scientific literature [8,10,11,18–20]

The emission measurements for Cs_2NaGaF_6 doped with 0.5 at% Cr^{3+} at 4.2 K are shown in Figs. 2a and b. In these spectra we have used the phase shift technique to distinguish the zero-phonon transitions for the two Cr^{3+} sites. In Fig. 2a, we have chosen the phase that gives the maximum intensity for the first line on the spectrum, located at 14,780 cm^{-1}. This is the magnetic dipole allowed zero-phonon line and corresponds to the $^2E \rightarrow {}^4A_2$ transition of Cr^{3+} ions at sites of octahedral symmetry. When we choose the phase that eliminates the zero-phonon transition at 14,780 cm^{-1} (Fig. 2b), only some lines situated at energies lower than 14,144 cm^{-1} remain on the emission spectrum. In this case, the sharp line at 14,144 cm^{-1} is a second zero-phonon line that also corresponds to the $^2E \rightarrow {}^4A_2$ electronic transition. In Ref. 10, these results and detailed arguments of symmetry allowed the correlation of the zero-phonon lines at 14,780 and 14,144 cm^{-1} with sites I and II, respectively. Consequently, the rich vibrational structure in Fig. 2b corresponds to the Cr^{3+} centers in site II. Moreover, when we compare the two spectra, we can identify the vibrational lines of the $[CrF_6]^{3-}$ complex that belong to site I.

It has been observed for other fluoride elpasolites containing complex anions that by far the most intense vibronic origins are formed by the odd internal vibrations of the complex anion [18]. The $t_{2u}(\pi)$ mode corresponds to a nonbonding orbital and must have the lowest difference of energy among all those possible. Moreover, the σ orbitals are symmetric with respect to rotation about the bond direction, while the π orbitals are not. So the position in energy of the $t_{1u}(\pi)$ mode is expected to lie higher than that of the $t_{1u}(\sigma)$ mode. By considering these observations for site I in $Cs_2NaGaF_6:Cr^{3+}$, the three strong vibronic peaks situated at 14,543 cm^{-1} (line 3), 14,489 cm^{-1} (line 4), and 14,257 cm^{-1} (line 8) can be assigned as the $t_{2u}(\pi)$, $t_{1u}(\pi)$, and $t_{1u}(\sigma)$ modes, respectively. We have observed another peak at 14,577 cm^{-1} (line 2), which is also attributed to the $t_{2u}(\pi)$ mode. In this case, we have considered the effect of the trigonal distortion of the Cr^{3+} site on the normal modes of the $[CrF_6]^{3-}$ complex. In fact, the *t* irreducible representations of the O_h group are reduced in $a + e$ irreducible representations of the C_{3v} group. Therefore, the $t_{2u}(\pi)$, $t_{1u}(\pi)$, and $t_{1u}(\sigma)$ modes are affected by the site distortion and they can have an additional degeneracy. This trigonal distortion explains the energy splitting, about 34 cm^{-1}, of the $t_{2u}(\pi)$ odd internal vibration.

The lines situated at 14,459, 14,347, and 14,269 cm^{-1} correspond to the $t_{2g}(\pi)$, $e_g(\sigma)$, and $a_{1g}(\sigma)$ modes, respectively, of the $[CrF_6]^{3-}$ complex in site I. For even vibrations, the t_{2g} mode is primarily a bending (π) mode and its frequency is expected to lie lower than that of the asymmetric e_g stretching (σ) mode, which in turn should lie below that of the symmetric a_{1g} stretching mode. The relatively high intensity of the $e_g(\sigma)$ line is not surprising when the Jahn–Teller effect is taken into account. This effect is more pronounced in *E* states than in *T*: the e_g orbitals are directed toward ligands and are more respondent to nonequivalency of interactions with the ligands than the t_{2g} orbitals, directed between ligands. Another possibility is the proximity of the ^2E_g and $^4T_{2g}$ states, which increases the degree of mixing of the energy levels. Furthermore, the observation of electric dipole allowed $e_g(\sigma)$ progressions on the three odd vibronic origins (lines 9, 10, and 14) gives other evidence for this assignment. The position of the $a_{1g}(\sigma)$ mode is more difficult to locate because it is close to the $t_{1u}(\sigma)$ vibrational mode. This mode is assigned to the shoulder on the high-energy side of the $t_{1u}(\sigma)$ vibrational origin, and, as well as the $e_g(\sigma)$ line, this attribution can again be confirmed by the combination of the $a_{1g}(\sigma)$ mode with the odd vibronic origins (lines 11, 13, and 15). For the $t_{2g}(\pi)$ mode, the position lies closer to $t_{1u}(\pi)$ than $t_{2u}(\pi)$, which agrees well with other hexafluoride complexes studied previously [6,19]. It is also observed that the $t_{2g}(\pi)$ vibronic mode adds on $e_g(\sigma)$, $a_{1g}(\sigma)$, and $t_{2u}(\pi)$, lines 12, 18, and 19, respectively, and probably forms progressions with $t_{1u}(\pi)$ and $t_{1u}(\sigma)$. The latter combinations cannot be observed because their expected energies are located directly beneath much more

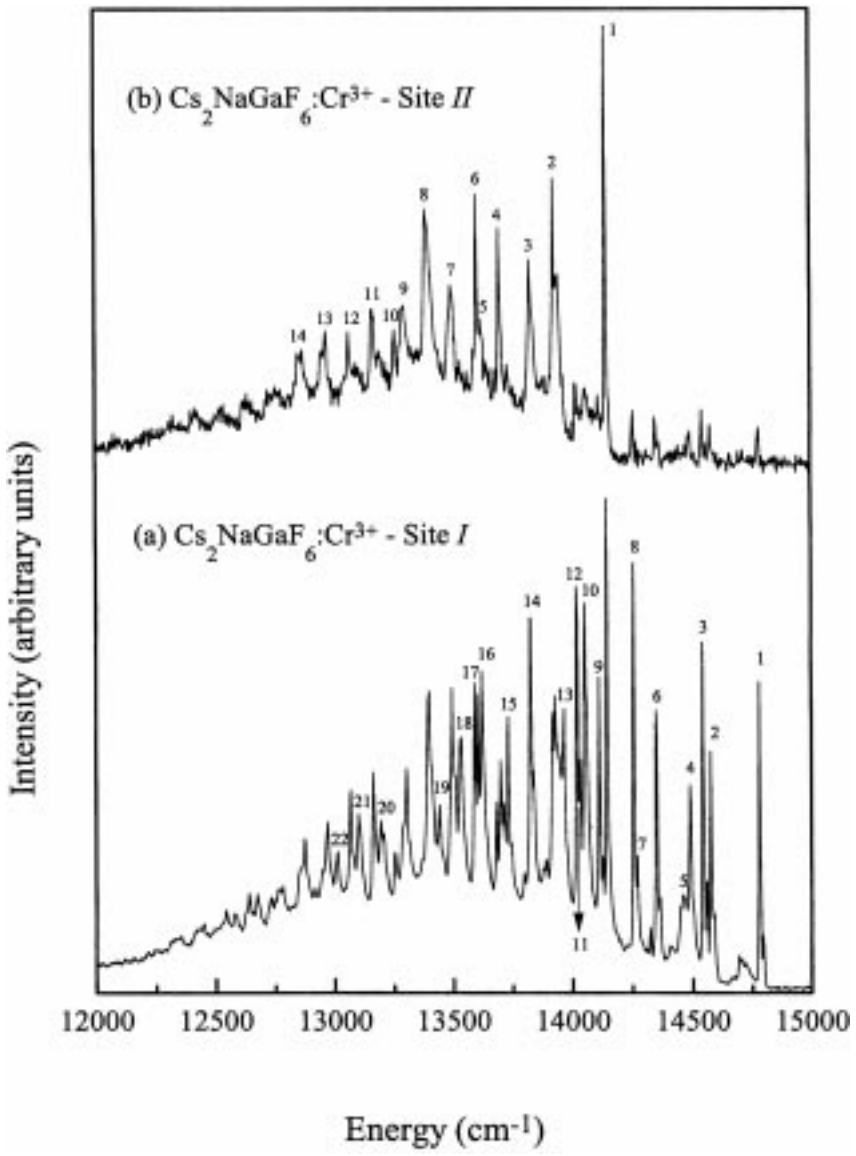

Fig. 2. Time-resolved emission spectra of Cs_2NaGaF_6 with 0.5 at% Cr^{3+} at 4.2 K with a phase shift that (a) maximizes and (b) eliminates the zero-phonon line at 14,780 cm^{-1}. The labeled peaks correspond to the vibrational lines of sites I and II, and their assignment is given in Table I.

intense lines. The results concerning site I are summarized in Table I.

A similar analysis is accomplished for the vibronic origins of the Cr^{3+} ions in site II of Cs_2NaGaF_6 (see Fig. 2b), and the assignment of these lines is also listed in Table I. The most significant difference in this spectrum is the disappearance of the $t_{2g}(\pi)$ mode. This can occur because the distortion caused by the introduction of the Cr^{3+} ion in site II is smaller than that in site I. This fact is confirmed by the absence of a second line associated with the $t_{2u}(\pi)$ mode, which appears when the trigonal effects are pronounced. As the t_{2g} electrons are little affected by small changes in their environment, the relative intensities of vibrational lines related to the transition of these electrons are very low. The combinations of the $a_{1g}(\sigma)$ and $e_g(\sigma)$ modes with the odd vibronic origins (lines 7 to 11) can also be observed in this spectrum, except for the $a_{1g}(\sigma) + t_{2u}(\pi)$ progression. When we use the values of the difference of energy of the two modes, this progression should be located at 13,404 cm^{-1}, close to the $t_{1u}(\pi) + e_g(\sigma)$ vibronic line. This proximity probably explains the enlargement of the latter.

Table I. Assignment of the Labeled Peaks for Sites I and II in $Cs_2NaGaF_6:Cr^{3+}$, with Their Energies and Frequencies

	$Cs_2NaGaF_6:Cr^{3+}$			
	Site I[a]		Site II[b]	
Line	ΔE (cm^{-1})	Assignment	ΔE (cm^{-1})	Assignment
1	0	Zero-phonon line	0	Zero-phonon line
2	203	$t_{2u}(\pi)$–C_{3v} distortion	216	$t_{2u}(\pi)$
3	237	$t_{2u}(\pi)$	317	$t_{1u}(\pi)$
4	291	$t_{1u}(\pi)$	445	$e_g(\sigma)$
5	321	$t_{2g}(\pi)$	524	$a_{1g}(\sigma)$
6	433	$e_g(\sigma)$	539	$t_{1u}(\sigma)$
7	511	$a_{1g}(\sigma)$	649	$t_{2u}(\pi) + e_g(\sigma)$
8	523	$t_{1u}(\sigma)$	754	$t_{1u}(\pi) + e_g(\sigma)$
9	668	$t_{2u}(\pi) + e_g(\sigma)$	846	$t_{1u}(\pi) + a_{1g}(\sigma)$
10	727	$t_{1u}(\pi) + e_g(\sigma)$	885	$2e_g(\sigma)$
11	747	$t_{2u}(\pi) + a_{1g}(\sigma)$	983	$e_g(\sigma) + t_{1u}(\sigma)$
12	763	$t_{2g}(\pi) + e_g(\sigma)$	1079	$a_{1g}(\sigma) + t_{1u}(\sigma)$
13	814	$t_{1u}(\pi) + a_{1g}(\sigma)$	1174	$a_{1g}(\sigma) + t_{2u}(\pi) + e_g(\sigma)$
14	956	$t_{1u}(\sigma) + e_g(\sigma)$	1294	$a_{1g}(\sigma) + t_{1u}(\pi) + e_g(\sigma)$
15	1048	$t_{1u}(\sigma) + a_{1g}(\sigma)$		
16	1160	$a_{1g}(\sigma) + t_{2u}(\pi) + e_g(\sigma)$		
17	1189	$a_{1g}(\sigma) + t_{2u}(\pi) + e_g(\sigma)$		
18	1245	$a_{1g}(\sigma) + t_{1u}(\pi) + e_g(\sigma)$		
19	1339	$2a_{1g}(\sigma) + t_{2g}(\pi)$		
20	1587	$2a_{1g}(\sigma) + t_{2g}(\pi) + t_{2u}(\pi)$		
21	1681	$2a_{1g}(\sigma) + e_g(\sigma) + t_{2u}(\pi)$		
22	1766	$2a_{1g}(\sigma) + e_g(\sigma) + t_{1u}(\pi)$		

[a] Zero-phonon line at 14,780 cm^{-1}.
[b] Zero-phonon line at 14,144 cm^{-1}.

In Fig. 3a we can observe the whole vibrational emission spectrum of Cs_2NaAlF_6 doped with 0.5 at% Cr^{3+} at 4.2 K. In this spectrum the emission at 14,249 cm^{-1} (line 1) was maximized by phase shift measurements. In fact, two zero-phonon lines are observed, at 14,890 and 14,249 cm^{-1}, and they correspond to the Cr^{3+} ions in sites I and II, respectively. Figure 3b shows the vibrational lines associated with site II, when the lines of site I are eliminated by phase shift. Site I has a lower symmetry than site II, and consequently, the $^2E \rightarrow {}^4A_2$ transition of Cr^{3+} centers occurs at a higher energy. Moreover, as for $Cs_2NaGaF_6:Cr^{3+}$, the comparison between Fig. 3a and Fig. 3b also allows us to distinguish the lines originating from site I and those from site II. Since the $^2E \rightarrow {}^4A_2$ electronic transition is electric dipole forbidden, the more intense vibronic lines are associated with odd internal vibrations of the complex anion, i.e., $t_{1u}(\pi)$ and $t_{2u}(\pi)$. As mentioned earlier, the decreasing order in frequency of the first vibronic modes is $t_{1u}(\sigma)$, $a_{1g}(\sigma)$, $e_g(\sigma)$, $t_{2g}(\pi)$, $t_{1u}(\pi)$, and $t_{2u}(\pi)$, and for site I, it is based on the electronic transition at 14,890 cm^{-1}.

The most intense internal vibration starts at the upper level $t_{2u}(\pi)$ and originates two close lines at 14,684 and 14,646 cm^{-1}, lines 2 and 3, respectively. This energy splitting is attributed to trigonal distortion at the Cr^{3+} site and its value is 38 cm^{-1}. The $t_{1u}(\pi)$ transition, at 14,586 cm^{-1} (line 4), presents one splitting at 14,594 cm^{-1}. This small energy difference, about 8 cm^{-1}, could be a trigonal distortion of the $t_{1u}(\pi)$ mode or a coupling between internal and lattice vibrational modes. The last mode relative to odd internal vibrational transitions, $t_{1u}(\sigma)$, is located at 14,355 cm^{-1} (line 7). Next to the $t_{1u}(\sigma)$ line we can see a shoulder on the higher-energy side, at 14,364 cm^{-1}, which is assigned to the symmelric $a_{1g}(\sigma)$ mode. Likewise, another peak can be observed, located at 14,556 cm^{-1} (line 5), which corresponds to the t_{2g} (π) mode. Finally, the asymmetric $e_g(\sigma)$ mode (line 6) is situated at 14,447 cm^{-1}. In Table II, we propose an attribution of the 26 vibronic lines labeled in Fig. 3a.

For site II, the observed vibronic origins are also listed in Table II. This assignment is, for higher-energy modes, analogous to that described above. As for the $Cs_2NaGaF_6:Cr^{3+}$ system, the exception is the $t_{2g}(\pi)$ mode, which is not observed for this site. In hexafluoride complexes the energy value of this mode is close to t_{1u} (π) [20] and its intensity is relatively low, which can mask the mode. From Table II, we can observe that the value of the structure of the vibrational levels for a given vibrational mode is very close in both sites. This fact shows that the structure of the levels is invariant, that is, although sites I and II have different symmetry characteristics, the emission $^2E \rightarrow {}^4A_2$ is the same. Both Cr^{3+} centers occupy sites near degeneracy of the $^4T_2$ (^4F) and ^2E (^2G) levels, and as this sample presents an absorption at the $^4T_2$ (^4F) level [11], the fluorescent radiation emitted by one site could be absorbed by the other one. In general these competitive processes can reduce the fluorescence efficiency, but this effect is minor in small, lightly doped samples.

When the spectra of the two Cr^{3+}-doped hexafluorides are compared, one can verify that the energy splitting of the $t_{2u}(\pi)$ mode associated with site I is larger in Cs_2NaAlF_6 than in Cs_2NaGaF_6. For site II, this splitting also occurs in $Cs_2NaAlF_6:Cr^{3+}$ but it is not present in the $Cs_2NaGaF_6:Cr^{3+}$ spectrum. Another interesting comparison concerns the t_{2g} (π) vibronic origin. This mode is well resolved in the spectrum of the aluminate (see Fig. 3a), while it is partially resolved in the gallate. Furthermore, we can observe that the positions in energy of the transitions in $Cs_2NaGaF_6:Cr^{3+}$ are less energetic than those in $Cs_2NaAlF_6:Cr^{3+}$. These results show that the sites occupied by Cr^{3+} ions have a lower symmetry in the latter lattice, which can be explained by the great

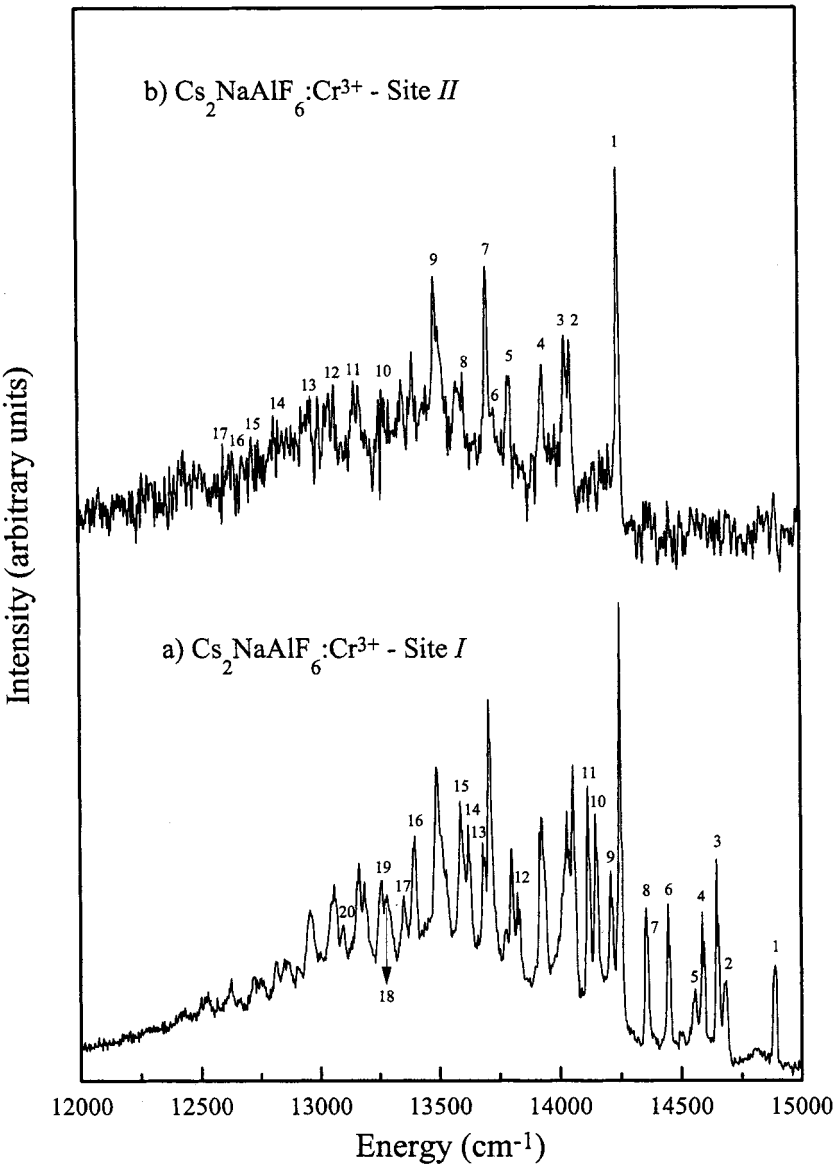

Fig. 3. Time-resolved emission spectra of Cs_2NaAlF_6 with 0.5 at% Cr^{3+} at 4.2 K with a phase shift that (a) maximizes and (b) eliminates the zero-phonon line at 14,890 cm^{-1}. The labeled peaks correspond to the vibrational lines of sites I and II, and their assignment is given in Table II.

difference between the ionic radii of Cr^{3+} and Al^{3+}, about 20%. In the gallate this difference is about 2%. In both Cr^{3+} sites of the aluminate and gallate, the high intensity of the a_{1g} and e_g progressions indicates that the degree of distortion of the ^2E state is much greater a long these coordinates. The $^4T_2$ level is also distorted along the a_{1g} and e_g coordinates because this state is strongly mixed with the ^2E level via spin-orbit interaction. Besides, as some t_{2g} (π) progressions are present for sites I of both materials, there is also a distortion of the ^2E and $^4T_2$ levels in this coordinate, which is clearly weaker than in the other two coordinates. However, the same distortion is not observed for sites II of Cs_2NaAlF_6:Cr^{3+} and Cs_2NaGaF_6:Cr^{3+}, probably due to the greater symmetry of these sites. These results agree well with those obtained in other hexafluoride compounds [18–21].

CONCLUSIONS

In this article, we have analyzed the vibrational transitions of the $[CrF_6]^{3-}$ complex in two slightly different sites of Cs_2NaGaF_6 and Cs_2NaAlF_6 single crystals. For both materials, the vibronic transitions have been identi-

Table II. Assignment of the Labeled Peaks for Sites I and II in $Cs_2NaAlF_6:Cr^{3+}$, with Their Energies and Frequencies

	$Cs_2NaGaF_6:Cr^{3+}$			
	Site I[a]		Site II[b]	
Line	ΔE (cm^{-1})	Assignment	ΔE (cm^{-1})	Assignment
1	0	Zero-phonon line	0	Zero-phonon line
2	206	$t_{2u}(\pi)$–C_{3v} distortion	196	$t_{2u}(\pi)$–C_{3v} distortion
3	244	$t_{2u}(\pi)$	220	$t_{2u}(\pi)$
4	304	$t_{1u}(\pi)$	310	$t_{1u}(\pi)$
5	334	$t_{2g}(\pi)$	444	$e_g(\sigma)$
6	443	$e_g(\sigma)$	513	$a_{1g}(\sigma)$
7	526	$a_{1g}(\sigma)$	543	$t_{1u}(\sigma)$
8	535	$t_{1u}(\sigma)$	640	$t_{2u}(\pi) + e_g(\sigma)$
9	681	$t_{2u}(\pi) + e_g(\sigma)$	761	$t_{1u}(\pi) + e_g(\sigma)$
10	742	$t_{1u}(\pi) + e_g(\sigma)$	951	$e_g(\sigma) + a_{1g}(\sigma)$
11	774	$t_{2u}(\pi) + a_{1g}(\sigma)$	1098	$2e_g(\sigma) + t_{2u}(\pi)$
12	1066	$t_{1u}(\sigma) + a_{1g}(\sigma)$	1181	$a_{1g}(\sigma) + t_{2u}(\pi) + e_g(\sigma)$
13	1210	$a_{1g}(\sigma) + t_{2u}(\pi) + e_g(\sigma)$	1279	$a_{1g}(\sigma) + t_{1u}(\pi) + e_g(\sigma)$
14	1270	$a_{1g}(\sigma) + t_{1u}(\pi) + e_g(\sigma)$	1415	$a_{1g}(\sigma) + 2e_g(\sigma)$
15	1303	$t_{1u}(\sigma) + a_{1g}(\sigma)$	1507	$a_{1g}(\sigma) + e_g(\sigma) + t_{1u}(\sigma)$
16	1496	$2a_{1g}(\sigma) + e_g(\sigma)$	1607	$a_{1g}(\sigma) + 2e_g(\sigma) + t_{2u}(\pi)$
17	1539	$a_{1g}(\sigma) + t_{2u}(\pi) + e_g(\sigma)$ $t_{1u}(\pi) + t_{2g}(\pi) + a_{1g}(\sigma)$	1645	$t_{1u}(\pi) + 3e_g(\sigma)$
18	1610	$+ e_g(\sigma)$		
19	1631	$2a_{1g}(\sigma) + t_{2g}(\pi) + t_{2u}(\pi)$		
20	1794	$2a_{1g}(\sigma) + e_g(\sigma) + t_{1u}(\pi)$		

[a] Zero-phonon line at 14,890 cm^{-1}.
[b] Zero-phonon line at 14,249 cm^{-1}.

fied from time-resolved emission spectra at low temperatures. It is observed that there are only small differences between the values of the vibrational modes of the two compounds and they agree well with the values found in other hexafluoride anions. These spectra also showed clearly that sites I and II for Cr^{3+} ions in Cs_2NaAlF_6 are more distorted than those in Cs_2NaGaF_6. Moreover, a detailed analysis of the vibrational structure observed leads to the conclusion that the ^2E and $^4T_2$ excited states are displaced along the e_g and a_{1g} coordinates for sites I and II in both materials. These states are also distorted along the t_{2g} coordinate for site I but not for site II. Additional experimental work is in progress to investigate the structural properties of these lattices by neutron diffraction. Moreover, the concentration dependence of the Cr^{3+} emission is being studied and it will be presented in another article.

ACKNOWLEDGMENTS

The authors wish to thank N. M. Khaidukov from the Institute of General and Inorganic Chemistry, Moscow, Russia, for providing the single crystal materials for the optical studies. R. J. M. da Fonseca, L. P. Sosman, and A. Dias Tavares Jr. acknowledge FAPERJ, FINEP, and CNPq for financial support. This work was also supported by DOE-BES (W-31.-109-ENG-38).

REFERENCES

1. S. A. Payne, W. F. Krupke, L. K. Smith, W. L. Kway, L. D. Deloach, and J. B. Tassano (1992) *IEEE J. Quant. Electron.* **28**, 1188–1196.
2. D. Welch, R. Craig, W. Streifer, and D. Scifres (1990) *Electron. Lett.* **26**, 1481–1483.
3. Harrison, A. Finch, D. M. Rines, G. A. Rines, and P. F. Moulton (1991) *Opt. Lett.* **1**, 581–583.
4. S. Kück, S. Hartung, S. Hurling, K. Petermahn, and G. Huber (1997) *Phys. Rev. B* **57**, 2203–2216.
5. H. N. Bordallo, G. F. Strouse, R. W. Henning, L. P. Sosman, R. J. M. da Fonseca, and A. Dias Tavares Jr. (2000) submitted for publication.
6. U. Sliwczuk, R. H. Bartram, D. R. Gabbe and B. C. McCollums (1991) *J. Phys. Chem. Solids* **52**, 357–361.
7. D. R. Lee, T. P. J. Han, and B. Henderson (1994) *Appl. Phys.* **A59**, 365–372.
8. M. Mortier, Q. Wang, J. Y. Buzaré, M. Rousseau, and B. Piriou (1997) *Phys. Rev. B* **56**, 3022–3031.
9. J. J. Adams, C. Bibeau, R. H. Page, D. M. Krol, L. H. Furu, and S. A. Payne (1999) *Opt. Lett.* **24**, 1720–1722.
10. R. J. M. da Fonseca, A. Dias Tavares Jr., P. S. Silva, T. Abritta, and N. M. Khaidukov (1999) *Solid State Commun.* **110**, 519–524.
11. L. P. Sosman, A. Dias Tavares Jr., R. J. M. da Fonseca, T. Abritta, and N. M. Khaidukov (2000) *Solid State Commun.* **114**, 661–665.
12. W. Massa and D. Babel (1988) *Chem. Rev.* **88**, 275–296.
13. E. Fargin, S. Lestienne, and J. M. Dance (1991) *Solid State Commun.* **75**, 769–771.
14. P. A. Tanner, L. Yulong, N. M. Edelstein, K. M. Murdoch, and N. M. Khaidukov (1997) *J. Phys. Condens. Matter* **9**, 7817–7822.
15. D. Babel and R. Haegele (1976) *J. Solid State Chem.* **18** , 39–45.
16. W. Demtröder (1982) in F. P. Schäfer (Ed.), *Laser Spectroscopy—Basic Concepts and Instrumentation*, Springer Series in Chemical Physics, Springer-Verlag, Berlin, pp. 547–585.
17. B. Di Bartolo (1968) *Optical Interaction in Solids*, John Wiley & Sons, New York, pp. 341–475.
18. C. Reber, H. U. Güdel, G. Meyer, T. Schleid, and C. A. Daul (1989) *Inorg. Chem.* **28**, 3249–3258.
19. J. Ferguson, H.J. Guggenheim, and D. L. Wood (1971) *J. Chem. Phys.* **54**, 504–507.
20. P. Greenough and A. G. Paulusz (1979) *J. Chem. Phys.* **70**, 1967–1972.
21. L. J. Andrews, S. M. Hitelman, M. Kokta, and D. Gabbe (1986) *J. Chem. Phys.* **84**, 5229–5238.